Analysis of FEL Radiation in Pulsed Raman Regime.

R. GIOVANELLI
Istituto di Scienze Fisiche dell'Università - 43100 Parma, Italia

(ricevuto il 6 Giugno 1994; approvato il 15 Novembre 1994)

Summary. — A direct numerical analysis, based on the Lienard-Wiechert potentials, is performed in the present paper, aiming to describe the relativistic interaction of the electrons composing a high-intensity beam (in Raman regime) both with each other and with the fields of an FEL structure and of an external resonant travelling electromagnetic wave. The different accelerations, due to the various forces acting on the charged particles, are seen to give different contributions to the total radiation field, which are separately considered here. The angular and frequency distributions of the obtained radiation are compared with the analytic ones deduced in the particular case of a single charge launched along the FEL structure. The interference effect between the fields of many bunches is seen to cause the shrinkage of the resulting radiation beam.

PACS 42.55.Tb – Free-electron lasers.
PACS 52.65 – Plasma simulation.
PACS 41.70 – Particles in electromagnetic fields (including synchrotron radiation).
PACS 41.80 – Particle beams and particle optics.

1. – Introduction.

Starting from a uniform electron beam injected along the axis of an FEL structure, the build-up of equispaced electron bunches is caused, as is well known, by an external resonant radiation (launched along the electron path) and hindered by the increasing electrostatic repulsion. Indeed the main effect of space-charge oscillations is to decrease the FEL performance by resisting the bunching of the electrons [1, 2], leading to a stimulated Raman backscattering with radiation frequency equal to the difference between the wiggler and the plasma frequency.

We try here to give an answer to the question whether and how the electrons not yet gathered by the bunches tend to be collected. This topic was partially treated in a previous work [3] (whose numerical methods are utilized here), where such a well-known tendency was confirmed.

In connection with this process we found it interesting, in the present paper, to analyse the radiation emitted both by the bunches and by the single electrons in terms of their different initial positions with respect to the bunches themselves.

The single-electron radiation turns out to be the sum of three contributions: a principal one, due to the FEL magnetic field, and two other ones, of different frequency spectrum and angular distribution. These latter contributions, although of quite smaller intensity, are present in angular and spectral ranges where the principal radiation is low, and may be therefore experimentally detected.

The first one of these two minor radiations is due to the particle acceleration caused by the external radiation, while the second one is due to the acceleration induced by the radiation coming from the bunches placed behind the considered particle.

Since therefore these two radiations are stimulated by other radiations, they turn out to be the part of the particle total radiation closest to the laser emission concept.

The angular distribution of these minor radiations tends to overlap on the principal radiation component when the particle is included in the nearest bunch. The experimental observation of these radiations could provide an interesting insight on the initial evolution of the bunches.

In our paper we analyse the non-stationary emission and interference pattern of the total radiation of few bunches collected by a screen placed at a finite distance from the FEL. We recall here that in the usual approach an ideal screen placed at infinite distance from an FEL structure entirely filled by stationary bunches collects the radiation pattern emitted only by a single charge [4].

We consider here, by means of the same numerical approach employed in [3], the evolution of a system composed of a limited number of macrocharges (bunches) in resonant condition, interacting through their radiation fields with a single charge moving in the FEL structure. Because of the coherent character of the resonant bunch radiation fraction directed along the FEL axis, the radiative behaviour of a bunch and of a particle receiving the bunch radiation strictly resembles that of a system of many (equispaced) bunches radiating on the considered test particle. At this stage no prediction can be made about the new FEL-gain curve.

To our knowledge a comprehensive display of the radiation patterns such as that presented in our work for non-stationary conditions, was never presented in previous papers.

Comparing the results presented here with those of the usual FEL theory (basically consisting in the description of the total power emission, phase lag between the external optical wave and the FEL radiation, electrostatic mutual forces, letargia and so on ...) a general agreement is found, integrated however by a deeper insight, visualizing also particle trajectories, of transient phenomena.

In sect. 2 a simplified analytical model is presented, allowing to give an approximated idea of the interference effects of the radiation emitted out of the FEL axis.

In sect. 3 numerical results are given for a single electron in an FEL. In sect. 4 numerical results are given for a charged particle interacting with the electromagnetic radiation coming from the FEL resonant bunches. In sect. 5 we consider the wave front deformation of the out-axis radiation, and its physical reason. Finally, in sect. 6, the radiation power spectrum, obtained in our numerical approach, is compared with the spectrum obtained by means of an analytic treatment of single charge in an FEL structure [4].

2. – A model for the approximation of the radiation emitted by a few bunches.

Although the numerical approach of the present paper does not necessarily require simplifying assumptions, we find it useful to present here a model retaining the essential physical points and showing the role played by interference phenomena arising when the radiation due to the different charges reaches a screen placed on the FEL axis.

Our model is based on the following simplifications:

a) The periodical displacement of the beam electrons from the straight trajectory is neglected.

b) A constant electron velocity along the FEL axis is assumed, coinciding with the actual average velocity $\bar{v}_x$ [3, 5]:

$$\bar{v}_x = \bar{\beta}_x c = c\left[1 - \frac{1 + a_w^2}{2\gamma^2}\right], \tag{2.1}$$

where $a_w = eB_w/\sqrt{2}\,k_w mc^2$ is the *interaction strength* [5],

$$\gamma^{-2} = 1 - \beta^2 , \qquad \boldsymbol{\beta} = \boldsymbol{v}/c , \qquad \beta^2 = \beta_x^2 + \beta_y^2 + \beta_z^2 ,$$

m is the electron rest mass, e is the electron electric charge, $k_w = 2\pi/\lambda_w$ is the wave number corresponding to the wiggler wavelength λ_w, and B_w is the wiggler magnetic strength:

$$\boldsymbol{B}_w(x) = -\hat{z} B_w \sin(k_w x) . \tag{2.2}$$

c) The transversal electron acceleration $\dot{\beta}_y c$ due to the magnetic wiggler field is computed making use of $\bar{v}_x$ alone:

$$\dot{\boldsymbol{\beta}} = -\hat{y} e \bar{\beta}_x B_w(x)/(m\gamma c) . \tag{2.3}$$

The maximum value of the transverse displacement neglected by our model may be shown [5] to be given by

$$y_{\max} = \sqrt{2}\cdot a_w/(k_w \gamma) . \tag{2.4}$$

Such a displacement may be therefore neglected for large enough values of γ and low enough values of the interaction strength a_w. The magnetic wiggler field B_w and the radiated electric field depend therefore essentially on the x-coordinate.

Let now imagine a sequence of bunches traveling along the x-axis equispaced by a distance x_1. Let

$$\lambda_R = \lambda_w(1 + a_w^2)/2\gamma^2 \tag{2.5}$$

be the resonant wavelength: the FEL emits therefore a radiation with such a wavelength when $x_1 = \beta\lambda_R$. The radiation arriving, at a certain time, at a point placed along the x-axis from a sequence of emitting electron bunches is originated by each bunch, at a previous time, from a position characterized by the fact that the field B_w is the same for all the bunches: this is the condition required by the coherency of the resulting radiation. For the radiated points P placed outside the axis x, however, destructive interference phenomena arise between the radiated fields, due to the

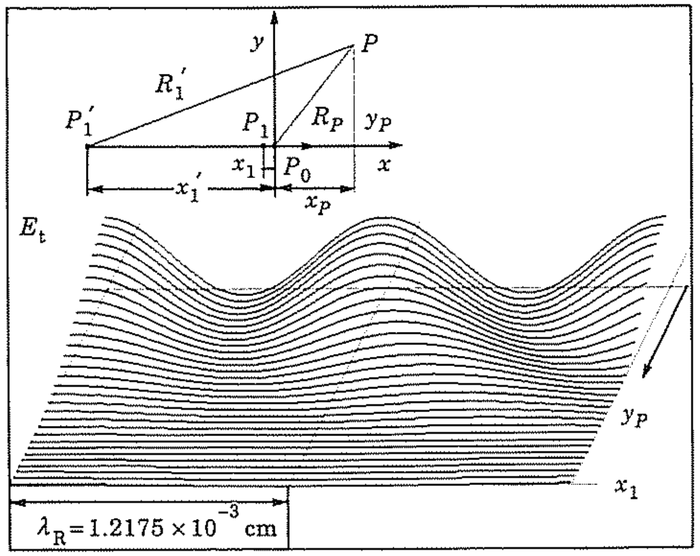

Fig. 1. – Scheme of the simplified model of the radiation distribution for a few bunches (see text for the symbols). The total radiated electric field E_t is calculated for 2 bunches. $\beta = 0.9995$, $x_P = 100$.

different values of the wiggler field computed at the new emitting positions. Let us now compute, within our model, the «previous positions», which we shall indicate by means of primed quantities.

Let x_P, y_P, z_P be the coordinates of the radiated point P (see fig. 1), and let $R_P = (x_P^2 + y_P^2 + z_P^2)^{1/2}$ be the distance between such a point and the first charge, initially placed at $x = 0$. The different radiations shall arrive at the position P at the same time ($T = 0$) provided that

$$R_n'/c + T_n' = R_P/c\,, \tag{2.6}$$

where $T_n' < 0$ is the previous time of the n-th charge and for $z_P = 0$

$$R_n' = (R_P^2 + x_n'^2 - 2x_P x_n')^{1/2} \tag{2.7}$$

is the distance between P and such a charge. Here

$$T_n' = (x_n' - n \cdot x_1)/(c\bar{\beta}_x) \tag{2.8}$$

and x_n' ($x_n' < 0$) is the relevant previous position of the n-th charge:

$$x_n' = T_n' c\bar{\beta}_x + n x_1\,. \tag{2.9}$$

From eqs. (2.7) and (2.9) T_n' is seen to be the solution of the equation

$$T_n'^2(1 - \bar{\beta}_x^2)c^2 + T_n' 2c \cdot (\bar{\beta}_x(x_P - n x_1) - R_P) - n^2 x_1^2 + 2x_P n x_1 = 0\,. \tag{2.10}$$

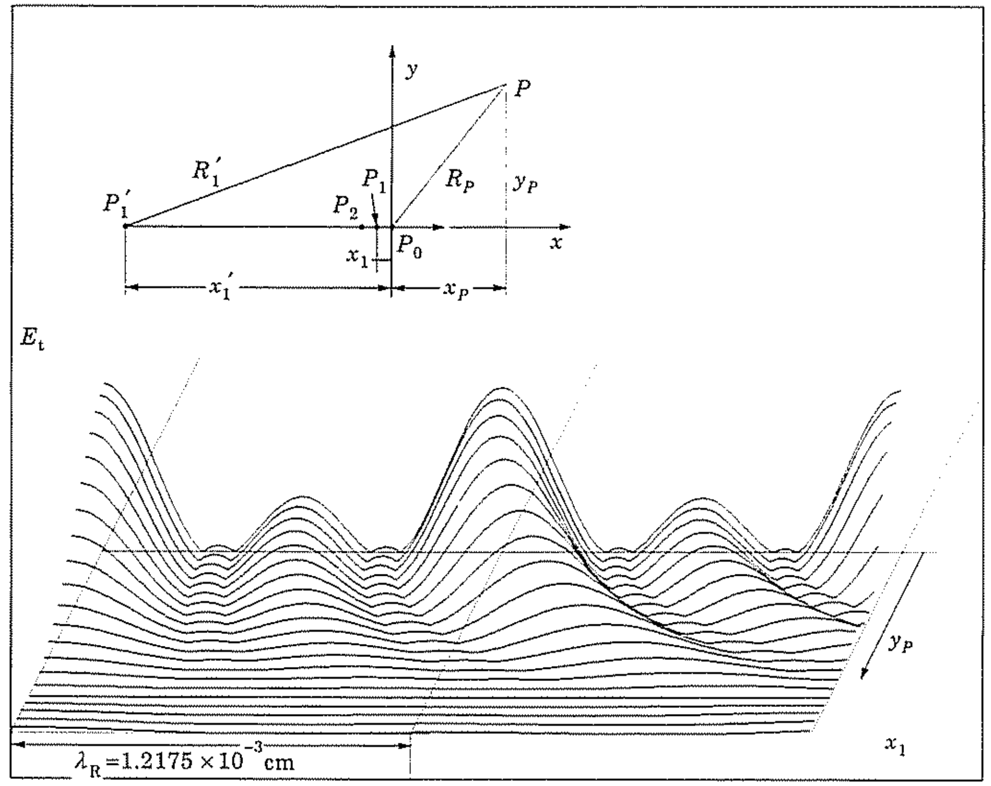

Fig. 2. – As in fig. 1, but for 3 bunches.

We have, therefore,

$$T_n' = \frac{(R_P - \bar{\beta}_x x_P + \bar{\beta}_x n x_1) \pm [R_P^2 + 2R_P\bar{\beta}_x(n x_1 - x_P) + \bar{\beta}_x^2 x_P^2 + n^2 x_1^2 - 2x_P n x_1]^{1/2}}{c(1 - \bar{\beta}_x^2)}\,,$$

where the negative sign must be adopted in order to have $T_n'(x_1 = 0) = 0$. If ϑ_n is the angle between the direction of R_n' and the x-axis, the total field arriving at P turns out to be mainly aligned along the y-axis and given [6] by

$$E_y = \frac{e\dot{\beta}_y \cos\vartheta_n(\cos\vartheta_n - \bar{\beta}_x)}{cR_n'(1 - \cos\vartheta_n \bar{\beta}_x)^3}\,.$$

We show in fig. 1, 2 and 3 the field E_y ($\equiv E_t$) due to the sum of the contributions of all the bunches as a function of x_1 and y_P for $z_P = 0$. For $y_P = 0$ field maxima are observed at $x_1 = n\lambda_R/N$ (where N is the number of bunches, and $n = 0, 1, 2, \ldots$), with absolute maxima for $n = kN$ ($k = 0, 1, 2, \ldots$).

The mutual distances between the field maxima increase for increasing values of y_P.

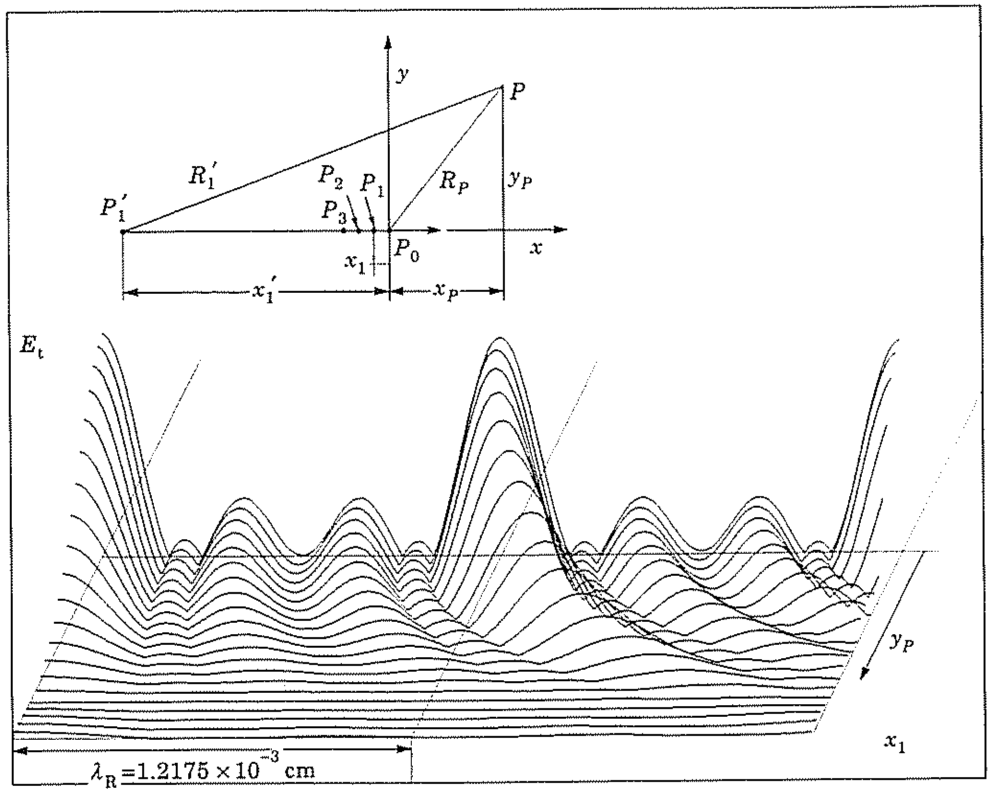

Fig. 3. – As in fig. 1, but for 4 bunches.

As we shall see, the radiation coming from a limited number of bunches turns out to be in substantial agreement, in our exact numerical solution, with the description provided by the simplified model introduced in the present section.

3. – Numerical solution of the exact motion and radiation equations.

Let us now analyse the results obtained when all the parameters of the particle motion are kept into account

In order to determine the positions from which the radiation, hitting the particle at a certain time, is originated, we shall refer to the actual trajectories of the entire particle system (fig. 4).

In the numerical computation the aforementioned positions shall be given by expressions analogous to eq. (2.6), where however R_n' shall depend on the effective particle trajectories; we shall therefore rewrite eq. (2.6), expressing each quantity in terms of the laboratory time T_n':

$$R_n'(x(T_n'),\, y(T_n'),\, T_n')/c + T_n' = R_P/c\,. \tag{3.1}$$

The results are summarized in fig. 5-7.

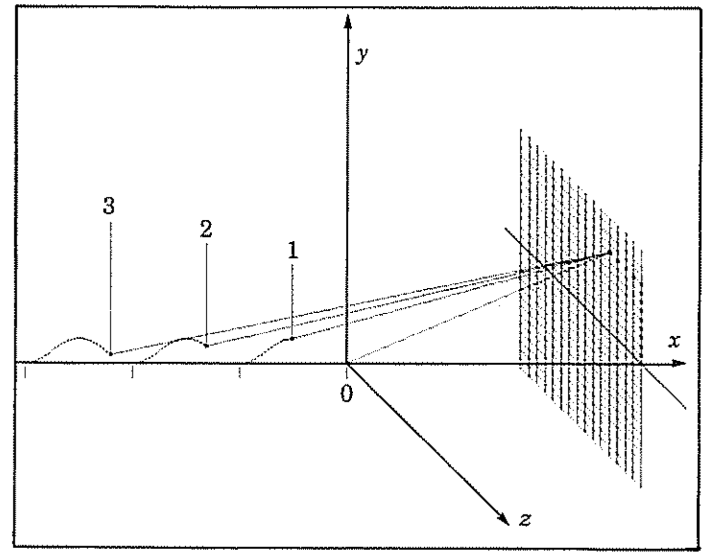

Fig. 4. – Scheme of the formation of the total radiation in an out-axis point of the screen. The sum is performed over the radiation fields (from the different FEL charges) reaching the point at the same time. Although the mutual distance between the charges at $t = 0$ is given by βL_R, their position at the earlier radiation time is quite different.

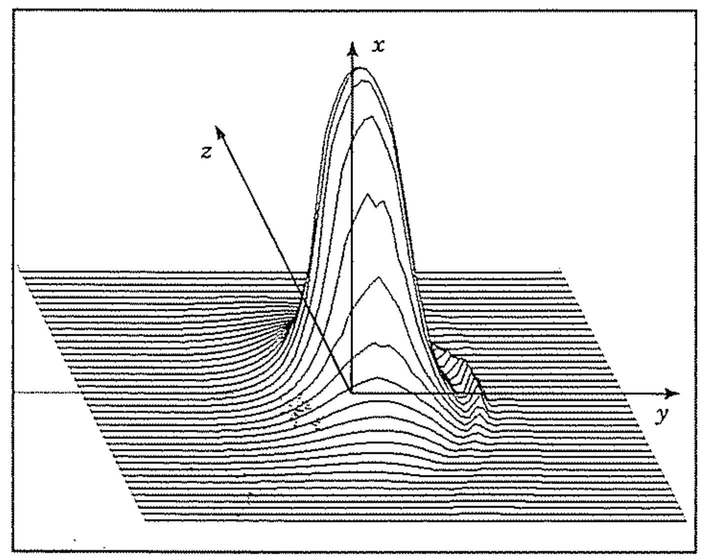

Fig. 5. – Electromagnetic radiation flux through a screen ($(20 \times 20)\ \text{cm}^2$) placed at 150 cm from the position P_0 of the first charge at $t = 0$. The radiation due to 2 bunches is the result of interference effects depending on the different charge position, as shown in fig. 4.

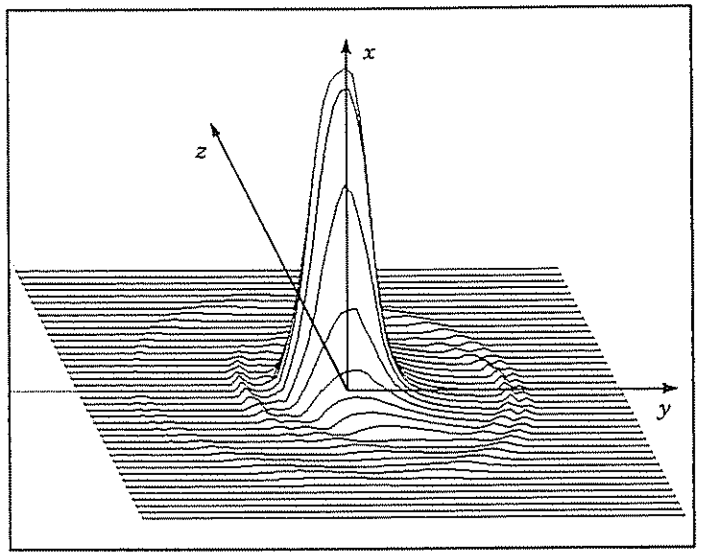

Fig. 6. – Analogous to fig. 5, except for the use of 4 bunches.

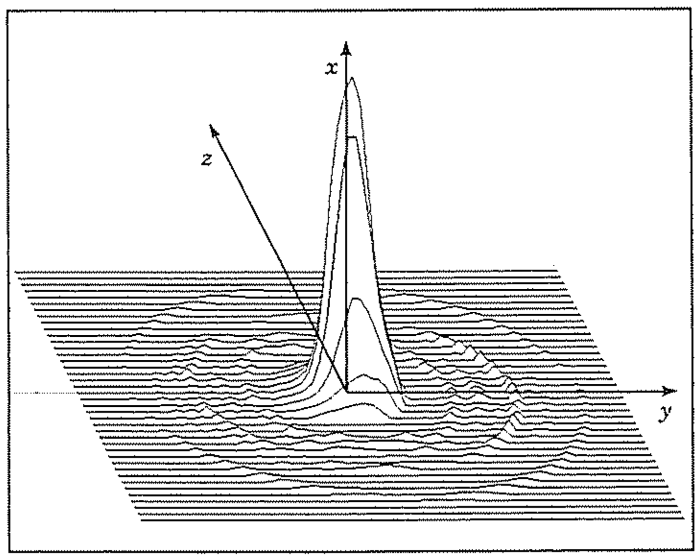

Fig. 7. – Analogous to fig. 5, except for the use of 7 bunches.

4. – Induced radiation.

The electric and magnetic fields emitted by a charge e moving with velocity $c\boldsymbol{\beta}$ and acceleration $c\dot{\boldsymbol{\beta}}$ may be expressed [7] in the form

$$\boldsymbol{E}(\boldsymbol{x}, t) = e\frac{(\hat{n} - \boldsymbol{\beta})(1 - \beta^2)}{\chi^3 R^2} + \frac{e}{c\chi^3 R}[\hat{n} \times \{(\hat{n} - \boldsymbol{\beta}) \times \dot{\boldsymbol{\beta}}\}], \tag{4.1}$$

$$\boldsymbol{B}(\boldsymbol{x}, t) = \hat{n} \times \boldsymbol{E}(\boldsymbol{x}, t), \tag{4.2}$$

where $\chi = (1 - \hat{n} \cdot \boldsymbol{\beta})$.

The fields are calculated in the actual position $\boldsymbol{x}$ of a point at a time t, and are radiated at t', that is R/c seconds earlier than the time t. The previous time t' is given by: $t' = t - R/c$, where the definition of R is analogous to the one given by eq. (2.6) for R_n' and $\hat{n}$ is the unit vector directed from the «retarded» position of the emitting charge (on the time t') toward the radiated point P (on the time t). While an analysis of the mutual radiation of two charges, based on the model of the previous section, was considered in ref. [3], we present now a more general description taking both the particle and the fields dynamics into account.

The acceleration $\dot{\boldsymbol{\beta}}$ of a particle (placed in P_0—fig. 8), with velocity $\boldsymbol{\beta}c$, interacting with electric and magnetic fields, is given by the general expression

$$\dot{\boldsymbol{\beta}} = \frac{e}{m\gamma c}[\boldsymbol{E} + \boldsymbol{\beta} \times \boldsymbol{B} - \boldsymbol{\beta}(\boldsymbol{\beta} \cdot \boldsymbol{E})]. \tag{4.3}$$

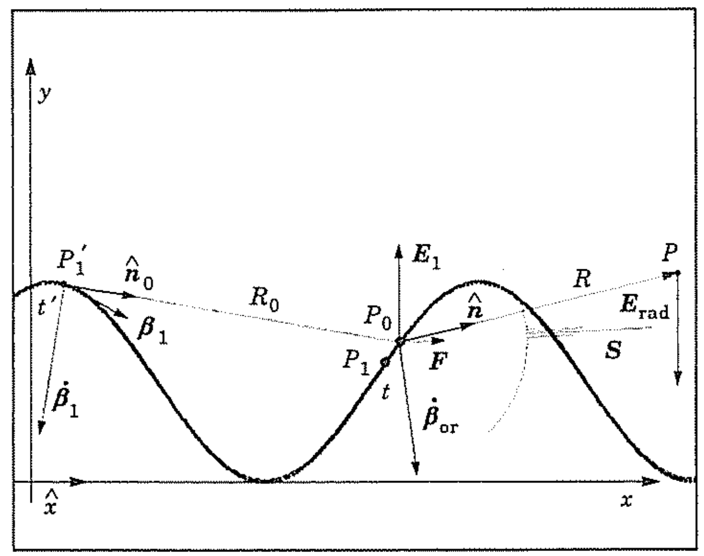

Fig. 8. – Radiative interaction between 2 charges. The radiation coming from the charge placed at P_1' (at the early time t') hits (generating a force F) the particle in P_0 at the time t.

If $\boldsymbol{B}$ and $\boldsymbol{E}$ are radiation fields (with $\boldsymbol{B} = \tilde{\boldsymbol{n}}_0 \times \boldsymbol{E}$), we have (for the particle in P_0 with acceleration $\dot{\beta}_0 c$ and velocity $\beta_0 c$)

$$\dot{\boldsymbol{\beta}} = \dot{\boldsymbol{\beta}}_{0\mathrm{r}} = \frac{e}{m\gamma_0 c}[\boldsymbol{E}(1 - \boldsymbol{\beta}_0\cdot\tilde{\boldsymbol{n}}_0) + (\tilde{\boldsymbol{n}}_0 - \boldsymbol{\beta}_0)(\boldsymbol{\beta}_0\cdot\boldsymbol{E})], \tag{4.4}$$

where $\tilde{\boldsymbol{n}}_0$ is the unit vector directed from the source (placed at P_1') to the radiated point (P_0).

Let us now recall that the total acceleration of a charge is due to the action of three different forces:

a) the force originated by the magnetic wiggler field (B_w);

b) the force impressed by the external electromagnetic wave (E_L, B_L) launched into the FEL;

c) the force due to the bunches (fields radiated E_1, B_1) following the radiated particle.

In agreement with this distinction we shall articulate the acceleration $\dot{\boldsymbol{\beta}}_0$ in

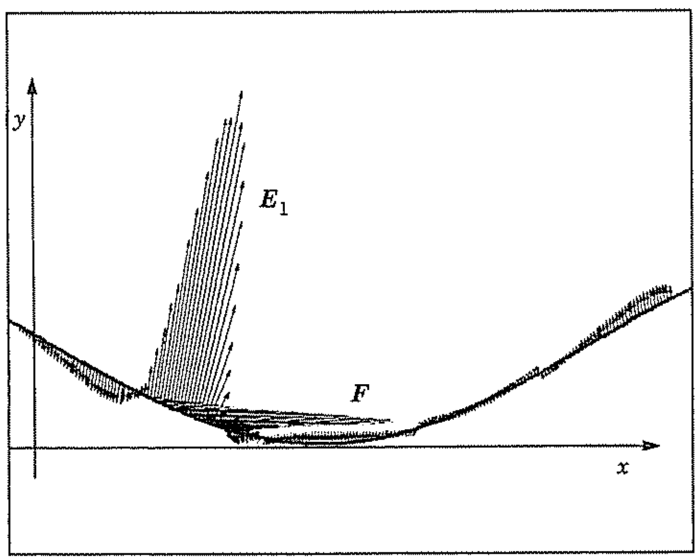

Fig. 9. – The arrows represent the electric field radiated by the charge placed in P_1' (fig. 8) on the one placed in P_0. Both charges are assumed to move along their trajectories. The transverse scale y is 50 times larger than the horizontal scale x.

the following three parts:

$$\begin{cases} \dot{\boldsymbol{\beta}}_{0\mathrm{w}} = \dfrac{e}{m\gamma_0 c}[\boldsymbol{\beta}_0 \times \boldsymbol{B}_\mathrm{w}], \\ \dot{\boldsymbol{\beta}}_{0\mathrm{L}} = \dfrac{e}{m\gamma c}[\boldsymbol{E}_\mathrm{L} + \boldsymbol{\beta}_0 \times \boldsymbol{B}_\mathrm{L} - \boldsymbol{\beta}_0(\boldsymbol{\beta}_0\cdot\boldsymbol{E}_\mathrm{L})], \\ \dot{\boldsymbol{\beta}}_{0\mathrm{r}} = \dfrac{e}{m\gamma_0 c}[\boldsymbol{E}_1(1 - \boldsymbol{\beta}_0\cdot\tilde{\boldsymbol{n}}_0) + (\tilde{\boldsymbol{n}}_0 - \boldsymbol{\beta}_0)(\boldsymbol{\beta}_0\cdot\boldsymbol{E}_1)], \end{cases} \tag{4.5}$$

where $\boldsymbol{E}_\mathrm{L}$ and $\boldsymbol{B}_\mathrm{L}$ are the external radiation fields.

In the absence of external radiation fields we have therefore

$$\dot{\boldsymbol{\beta}}_0 = \dot{\boldsymbol{\beta}}_{0\mathrm{w}} + \dot{\boldsymbol{\beta}}_{0\mathrm{r}}.$$

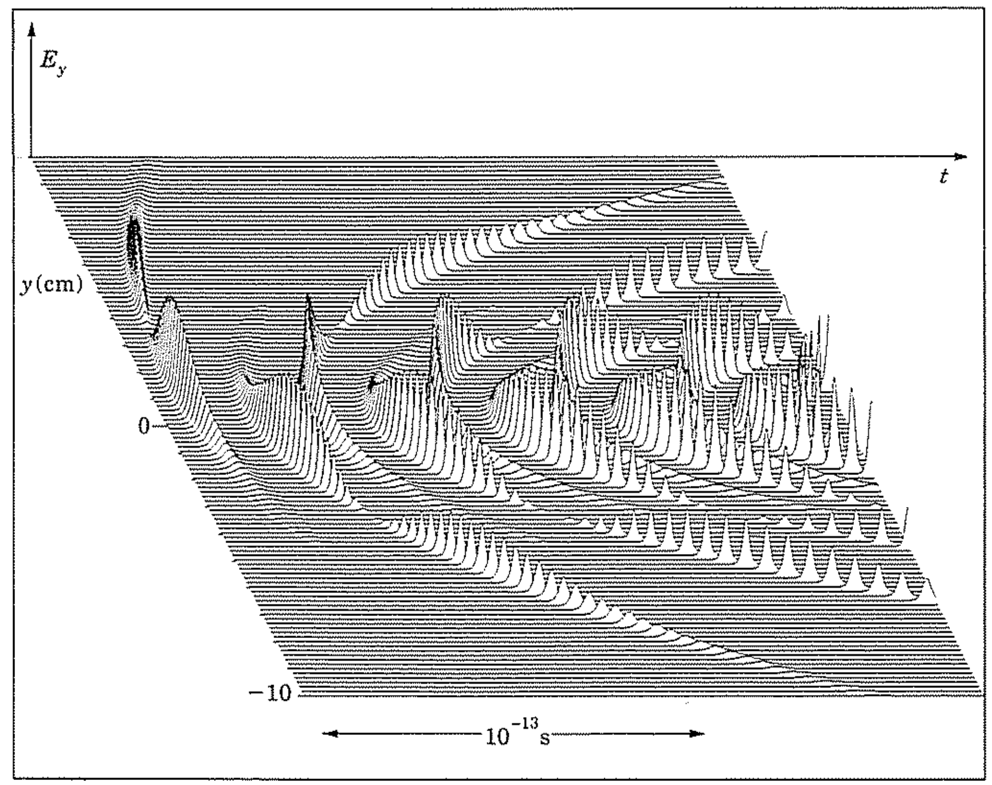

Fig. 10. – The electric-field component E_y of the induced radiation is plotted on the plane (y, t) in order to represent the progressive curvature increment of the wave fronts in terms of the curvature difference from the first one, the first wave front is assumed to be flat.

Referring to fig. 8 and 9, the electric field $\boldsymbol{E}_1$, due to the bunch placed in P_1', is given by

$$\boldsymbol{E}_1 = \frac{ke}{cR_0\chi_1^3}\,\bar{\boldsymbol{n}}_0 \times [(\bar{\boldsymbol{n}}_0 - \boldsymbol{\beta}_1)\times\dot{\boldsymbol{\beta}}_1], \tag{4.6}$$

where $\chi_1 = (1 - \bar{\boldsymbol{n}}_0 \cdot \boldsymbol{\beta}_1)$, k is the number of electrons contained in a generic bunch, and $\bar{\boldsymbol{n}}_0$ is the unit vector along the direction $\overline{P_1' P_0}$. Recalling now that

$$\boldsymbol{\beta}_1 = \bar{x}\beta_{1x} + \bar{y}\beta_{1y}; \qquad \boldsymbol{\beta}_0 = \bar{x}\beta_{0x} + \bar{y}\beta_{0y}; \qquad \dot{\boldsymbol{\beta}}_1 = \bar{x}\dot{\beta}_{1x} + \bar{y}\dot{\beta}_{1y};$$

and approximating $\bar{\boldsymbol{n}}_0 \cong \bar{x}$, we obtain

$$\boldsymbol{E}_1 = \frac{ke}{cR_0\chi_1^3}\,\bar{y}[\dot{\beta}_{1y}(\beta_{1x} - 1) - \beta_{1y}\cdot\dot{\beta}_{1x}], \tag{4.7}$$

from which we get, using eq. (4.5),

$$\dot{\boldsymbol{\beta}}_{0r} = \frac{E_1 e}{m\gamma_0 c}[\bar{x}\beta_{0y}(1 - \beta_{0x}) + \bar{y}(1 - \beta_{ox} - \beta_{0y}^2)]. \tag{4.8}$$

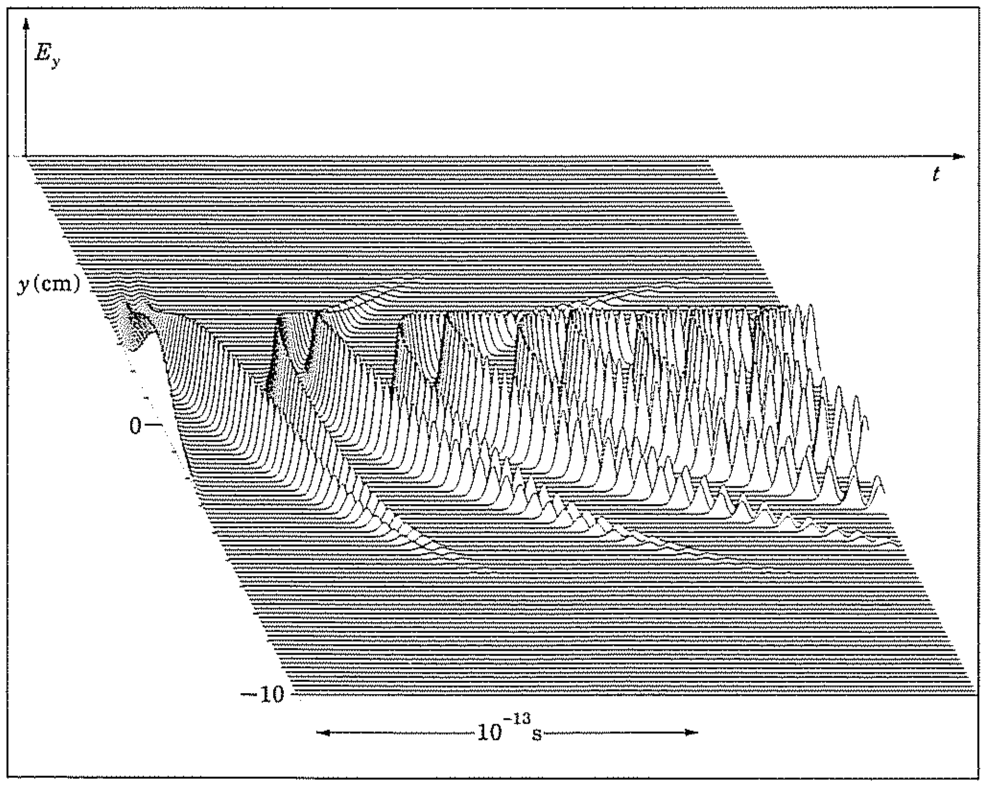

Fig. 11. – Plot of the electric-field component of the principal radiation due to a single charge, in the same conditions of fig. 10, but with a vertical scale 10^3 times smaller.

We have, therefore,

$$\boldsymbol{E}_{\text{rad}} = \frac{e}{cR\chi_0^3}\,\bar{\boldsymbol{n}} \times [(\bar{\boldsymbol{n}} - \boldsymbol{\beta}_0)\times\dot{\boldsymbol{\beta}}_{0r}], \tag{4.9}$$

where $\chi_0 = (1 - \bar{\boldsymbol{n}}\cdot\boldsymbol{\beta}_0)$. Equation (4.9) provides a radiation electric field lower than the one due to the action of the wiggler magnetic field by almost three orders of magnitude, leading therefore to a radiated power 10^{-6} times smaller (see fig. 10, 11). Due to the fact that its frequency range and angular distribution are different and separated by the main FEL radiation, such a field, however, may be detected and utilized for the description both of the bunch formation and the FEL instabilities.

5. – Deformation of the wave front.

The angular distribution of the radiation emitted by an accelerated charge may be calculated [1, 5, 8, 9] using eqs. (4.1) and (4.2) and the values of $\boldsymbol{x}(t)$, $\boldsymbol{\beta}(t)$, $\dot{\boldsymbol{\beta}}(t)$ obtained from the numerical integration of the motion equation. The wave front of such a radiation has a curvature radius equal to the distance R between the retarded position of the radiating charge and the observation point. We take here into account, for simplicity sake, only the dominant component (directed as $\bar{y}$) of the wave electric field $\boldsymbol{E}$. When the bunches are equispaced at resonant distances λ_R the total radiation emitted along $\bar{x}$ is obviously coherent, but it loses its coherence when observed along a direction even slightly different from $\bar{x}$, because the radiation, coming from the different charges (or bunches) in their new retarded positions, has a different phase for each charge, as shown by the simplified model. The wave shape, moreover, is symmetrical with respect to $\bar{x}$ only on the plane (x, z), out of which the symmetry is progressively lost, as we shall now see in detail. This asymmetry effect is known and described in previous literature [4], without, however, reaching a full understanding of its physical reason, which we shall stress in the following.

When, in the resonant case, a charge passes through the point 1 at $t = 0$, a second charge, following the first one at a distance $\beta\cdot\lambda_L$, passes through 1 at the later time $t = \beta\lambda_L/\beta c$.

Let now (fig. 12): P be an observation point outside the axis $\bar{x}$; θ be the observation angle between $\bar{x}$ and the line connecting the radiating charge with P; R_1, R_2 be the distances between P and the points 1 and 2, respectively; θ_1, θ_2 be the values of θ when the emitting charge is at the point 1 and 2, respectively (for R_1, R_2 large it shall be $\theta_1 \cong \theta_2$). Let us introduce moreover the wavelengths $\lambda_L(\theta_1) \equiv \lambda_L^\theta$ observed at P when the emitting charge is passing from the point 1 to the point 2.

$\lambda_L(\theta = 0)$ is the wavelength observed at any point of the $\bar{x}$-axis (being $\lambda_L(0) = \lambda_R$). It is easily seen that

$$\begin{cases} R_1 - R_2 \cong \lambda_w \cos\theta_1; \\ \lambda_L(\theta_1) - \lambda_L(0) = R_2 + \lambda_w - R_1 = \lambda_w(1 - \cos\theta_i) \cong \lambda_w\theta_1^2/2. \end{cases} \tag{5.1}$$

The wavelength λ_L is a function only of the observation angle θ, and does not depend

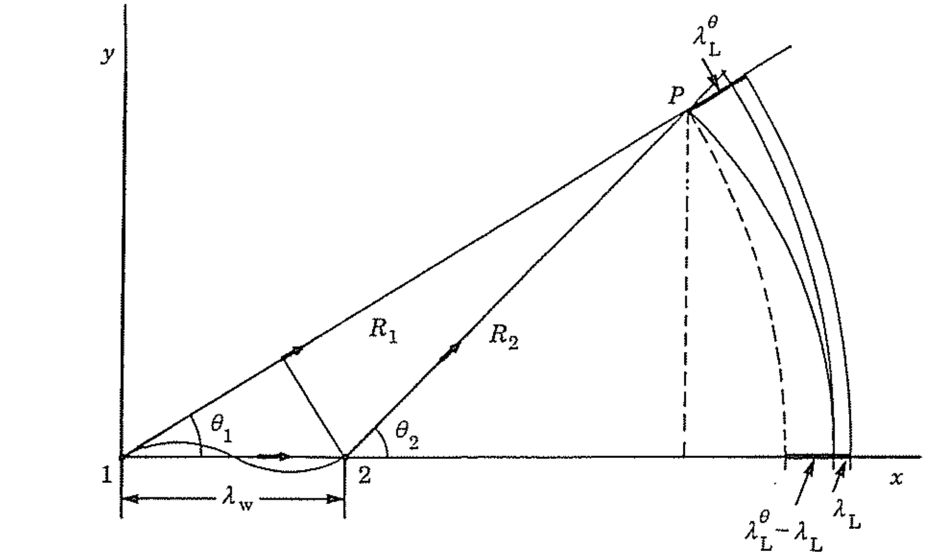

Fig. 12. – Scheme of the wavelength increment of the radiation due to a single charge, as a function of the observation angle θ. The wavelength for $\theta = 0$ is given by: $\lambda_L = \lambda_w(1 - \bar{\beta}_x)/\bar{\beta}_x$. The wavelength of the radiation emitted by the same charge, when it passes from the point 1 to 2, is given by: $\lambda_L^\theta \equiv \lambda_L(\theta) \cong \lambda_L + \lambda_w \theta_1^2/2$.

on the distance R. If P is not at infinity the angle θ shall obviously increase during the particle motion. The wavelength spectrum observed at P shall therefore range between the values

$$\lambda_L(\theta_i) = \lambda_R + \lambda_w \theta_i^2/2 \qquad \text{and} \qquad \lambda_L(\theta_o) = \lambda_R + \lambda_w \theta_o^2/2\,,$$

θ_i and θ_o being the values of θ corresponding, respectively, to the input and output section of the wiggler. The space and time distribution of the radiated electric-field component E_y is represented in fig. 13, 14, assuming $R_1 = \infty$ at the initial wave front, and plotting the R variation of the following wave fronts. The wave front curvature $(1/R)$ is seen to increase progressively during the particle motion.

We represent in fig. 15 a length λ_w along the particle trajectory (corresponding to a wiggler period along which a complete radiation wavelength is emitted) schematizing the actual almost sinusoidal by means of the straight lines 1^-2 and 2^-3. Another simplification consists in assuming the line 1^-2 directed along R_1. Both along 1^-2 and 2^-3 the velocity βc is assumed to be constant. Since

$$R_1 - R_2 = \lambda_w/(2\cos\theta) \qquad \text{and } R_2 - R_3 = \cos(2\theta)\,\lambda_w/(2\cos\theta)\,,$$

we have

$$(t_2 - t_1)\,c = R_2 + (R_1 - R_2)/\beta - R_1 = \lambda'_w\left[\frac{1}{\beta} - 1\right]\frac{1}{2}$$

and

$$(t_3 - t_2)\,c = R_3 + (R_1 - R_2)/\beta - R_2 = \lambda'_w\left[\frac{1}{\beta} - \cos(2\theta)\right]\frac{1}{2}\,,$$

with $\lambda'_w = \lambda_w/\cos\theta$.

The time intervals corresponding, respectively, to the first- and second-half

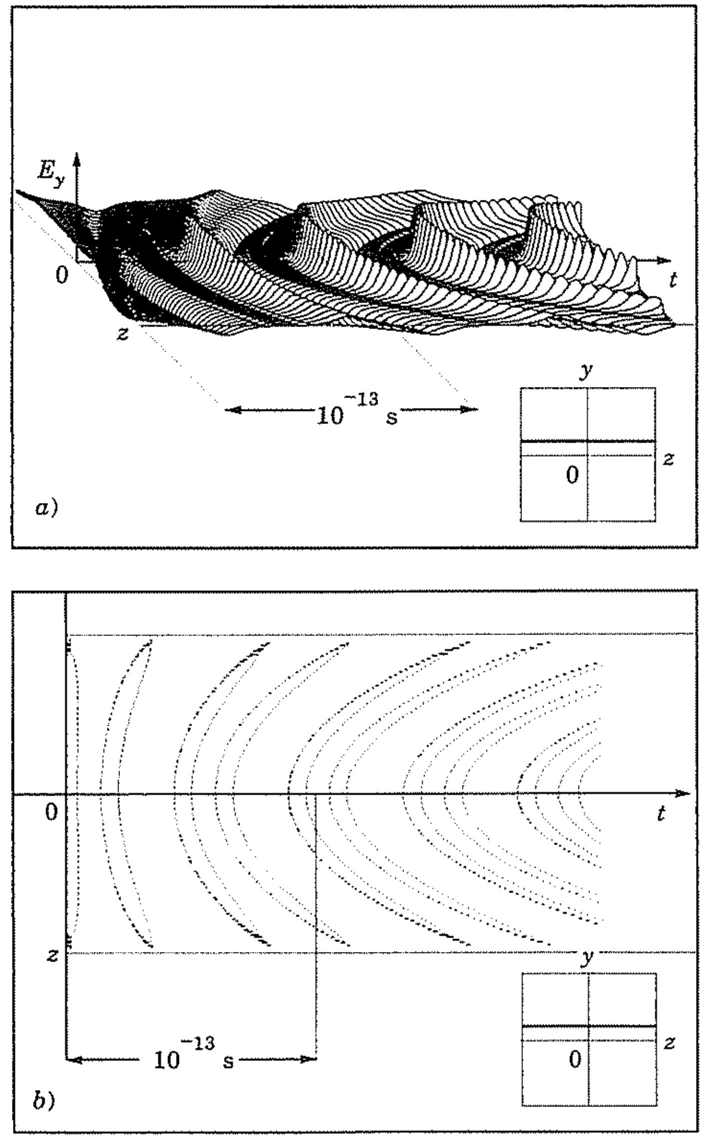

Fig. 13. – a) Axonometry of the wave fronts of the radiated electric field represented assuming in the figure an initially flat wave front. The represented radiation is that collected along the vertical thick line in the screen of (20×20) cm^2 placed on the (y, z)-plane at 300 cm from the orbit starting point. b) The same wave fronts represented by a view of the (y, t)-plane with two contour lines per wave.

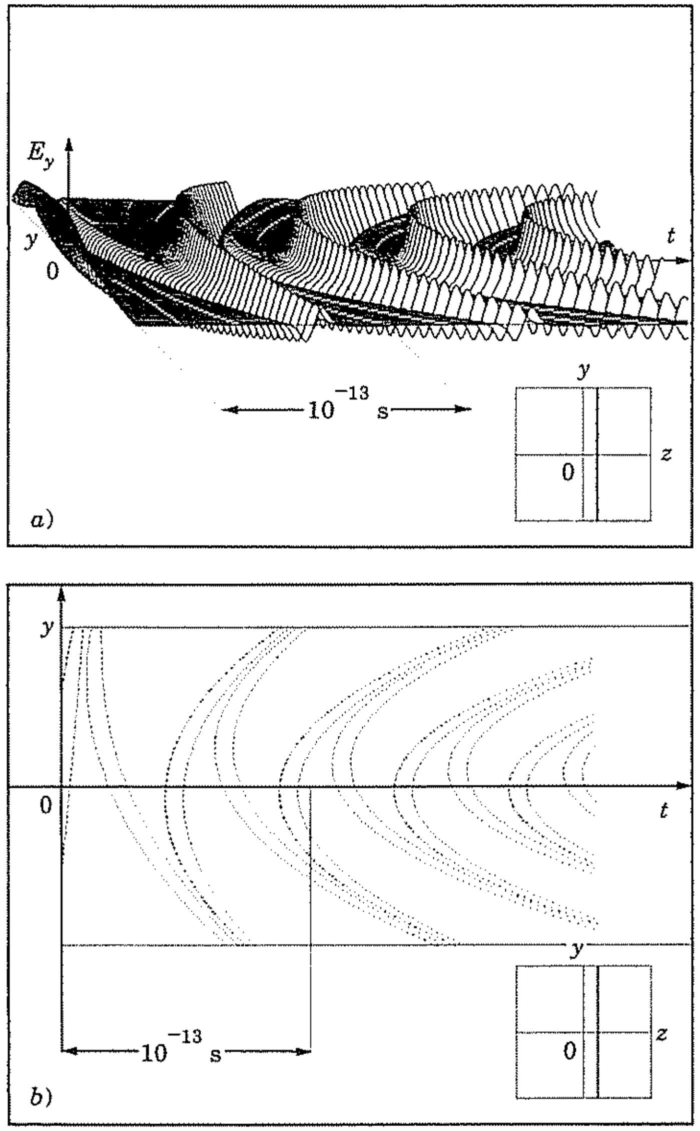

Fig. 14 – *a*) The same as in fig. 13*a*) for a horizontal collecting line. *b*) As in fig. 13*b*) the same wave fronts of *a*) are represented by a view of the (z, t)-plane.

wavelength turn out, therefore, to be different, leading to a deformation of the wave shape seen in P, although the total wavelength $\lambda_L(0)$ is always given by eq. (5.1). The geometry of this phenomenon is not symmetric with respect to the axis $\hat{x}$: the distortion is different if the point P lies on the positive or negative side of $\hat{y}$-axis. This is shown in fig. 13*a*), representing the axonometry of the wave fronts of the radiated electric-field component E_y, collected along a line parallel to the $\hat{y}$-axis.

In order to have the possibility of representing the progressive curvature modification of the wave fronts in terms of the curvature difference from the first one, in fig. 13*a*) we assume flat the first wave front.

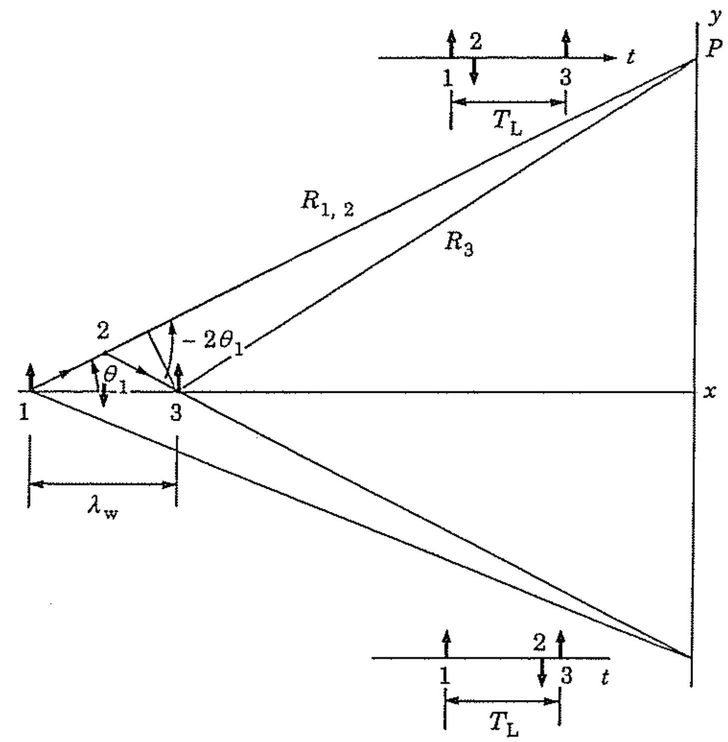

Fig. 15. – Schematic representation of the particle trajectory, corresponding to a wiggler step λ_w along which a complete radiation wavelength is emitted. The wavelength is not symmetric if the radiation is seen in the plane (x, y) to the direction of the wiggler magnetic field.

In fig. 13*b*) the same wave fronts are projected on the plane (y, t). As we shall see in the next section, the aforementioned wave front deformation strongly affects the spectrum of the out-axis radiation emitted on the plane containing the particle trajectory.

Figures 14*a*) and *b*) are analogous to fig. 13, with a collecting line parallel to the $\hat{z}$-axis.

6. – Electromagnetic-radiation spectrum.

The method we employ to obtain the radiation angular distributions and its frequency spectrum is based on the numerical solution of the general radiation equation, on the actual electron trajectories, and on the fast Fourier analysis of the emitted radiation.

This procedure allows to evaluate the field error, fringe fields, and near-field effects.

The relativistic particle radiation is confined within a forward cone of angular width $\sim \gamma^{-1}$, with axis directed as the particle velocity. If the maximum transverse displacement y_{max} (eq. (2.4)) is large enough, the radiation cone will periodically be deflected out of a detector placed at infinity on the $\hat{x}$-axis. This will cause radiation from many harmonics to appear (up to $\sim \gamma^3$ times the fundamental) and produce a broad band of frequencies. The requirement for the detector to stay in the radiation cone is $y_{\max}/\gamma^{-1} \leqslant 1$.

Because of the complexity of the interference distribution, the analytical study of the real angular distribution of the radiation emitted by a whole FEL is quite difficult (see fig. 16*a*), *b*)). The analytical treatment of the radiation produced by a single electron is the basis to describe the radiation of an electron beam, starting from the phase space distribution function of the electrons and from the «addition theorem» [9] of the radiation fields. The results of such a calculation provide the emission spectra

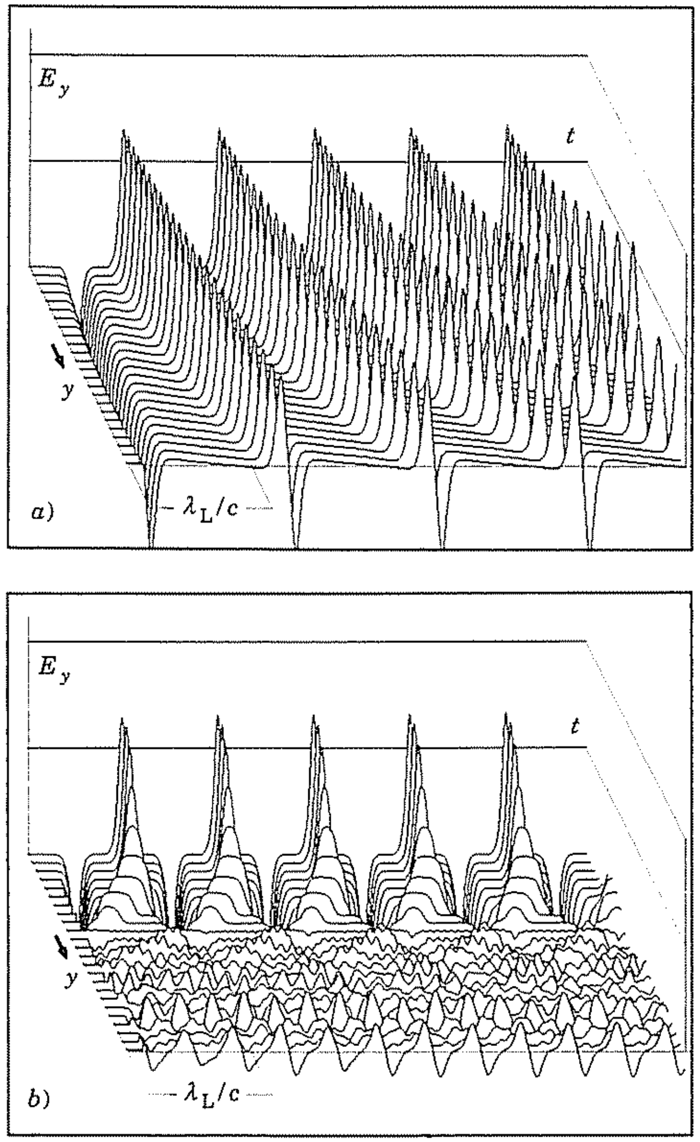

Fig. 16. – *a*) Electric-field component E_y radiated by a single charge traveling with kinetic energy of 13.1 MeV in an FEL with $\lambda_w = 2$ cm and peak magnetic field of 5500 G. *b*) The same as *a*), for the case of 14 charges at mutual resonant distances $\beta\lambda_L$.

allowing to optimize the syncrotron radiation generated by a wiggler (or undulator) inserted along the path of the high-energy electrons of a storage ring. In order to include the effects of the entire electron beam emittance [10], one must perform a convolution between the phase space distribution of the undulator radiation due to a single particle, with the phase space distribution of the entire electron beam, composed of statistically independent electrons. The total radiated electric field is calculated in the form of the Wigner distribution [11], as developed by Kim [9].

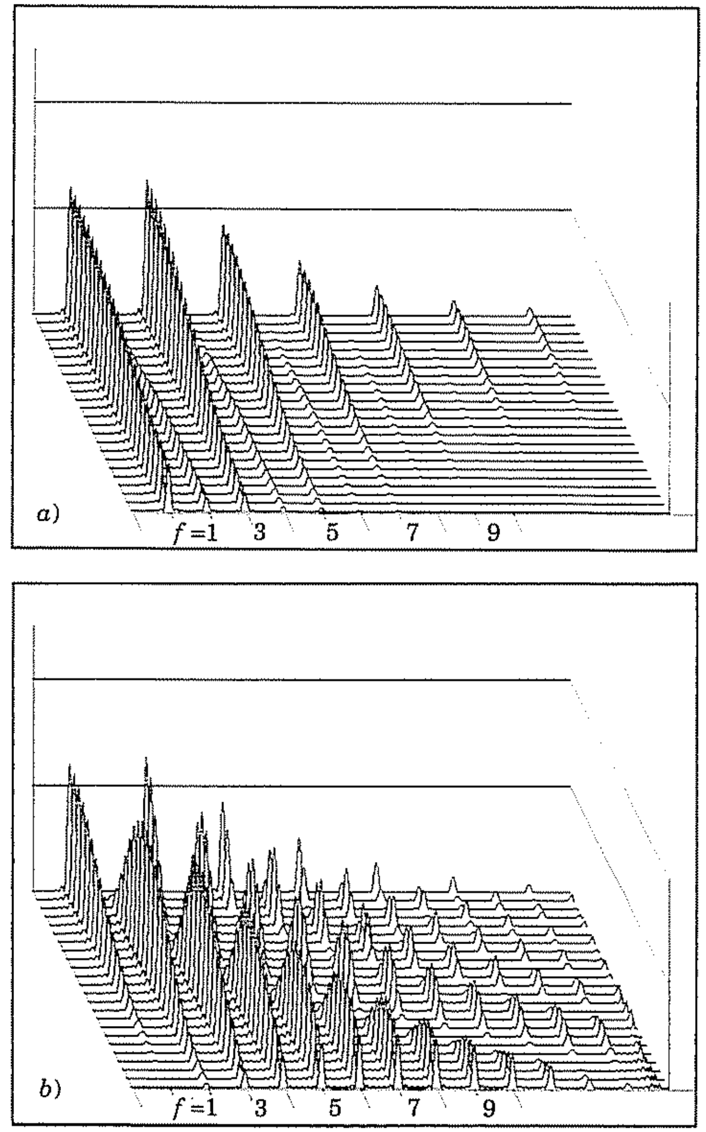

Fig. 17. – Spectral analysis of the radiation corresponding to fig. 16*a*), performed by means of an analytical approach [4]. The observation angle θ ranges between zero and 0.046 rad. A seven-period wiggler has been employed. The observation angle is assumed on a plane perpendicular to the wiggler magnetic field in *a*), and parallel to such a field in *b*).

The numerical technique adopted in the present work could be applied, with a treatment quite simpler than the one using the convolution approach, even to the harmonic analysis of the off-axis FEL radiation due to many bunches. We show in fig. 19 a typical example of such a radiation analysis in the case of bunches at resonant mutual distances.

In order to compare the standard analytical results [4, 12], holding on the case of a single particle, with our general numerical techniques, let us previously outline the basic points of the analytical approach.

The energy emitted by a single electron into a frequency interval $d\omega$ and a solid

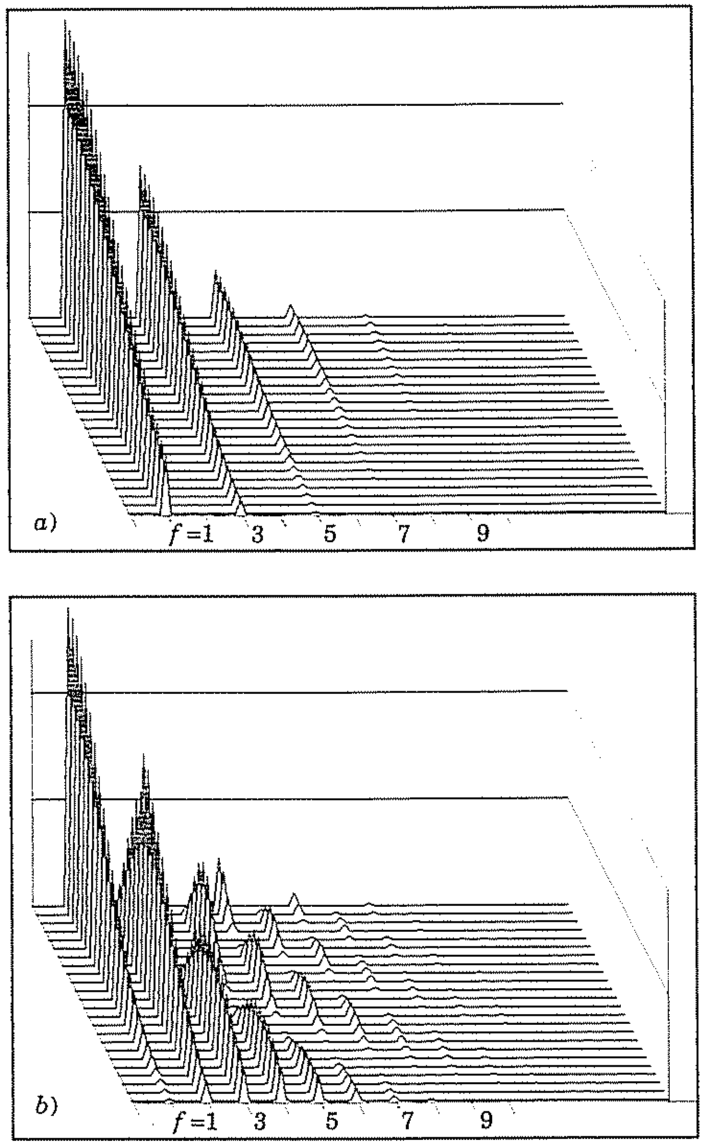

Fig. 18. – Spectral analysis analogous to fig. 17, obtained however using our numerical approach.

angle $d\Omega$ using the well-known Lienard-Wiechert integral is given by [7]

$$\frac{d^2 I}{d\omega\, d\Omega} = \frac{e^2\omega^2}{4\pi^2 c}\left|\int_{-\infty}^{\infty} \hat{n}\times(\hat{n}\times\boldsymbol{\beta})\exp[i\omega(t-\hat{n}\cdot\boldsymbol{r}(t)/c)]\,dt\right|^2, \tag{6.1}$$

where $\boldsymbol{r}(t)$ is the vector describing the path of the electron, $\boldsymbol{\beta}(t) = \dot{\boldsymbol{r}}(t)/c$, and $\hat{n}$ is a unit vector pointing from the origin of coordinates (chosen at the centre of the FEL) to the observer.

Reference [4] computes the integral contained in eq. (6.1), making use of simple analytical expressions of $\boldsymbol{r}(t)$ and $\boldsymbol{\beta}(t)$. The effective limits of the time integral are found observing that the electron radiation is originated only within the wiggler length $L = N\lambda_w$ (where N is the number of magnetics periods), and therefore for a time $L/\beta c$.

Each resonant term of the electromagnetic emission [4] is centred about the corresponding radiation frequency ω_θ, satisfying the equation

$$\omega_\theta = \omega_w f/(1-\bar{\beta}_x\cos\theta), \tag{6.2}$$

where θ is the observation angle away from the FEL axis $\hat{x}$ (such that $\cos\theta = \hat{n}\cdot\hat{x}$), f is the harmonic number, and $\omega_w \cong 2\pi c/\lambda_w$.

Equation (6.2) can be derived, for $f = 1$, from eq. (5.1) (see fig. 12), observing that $\omega_\theta = 2\pi c/\lambda_L^\theta$, with

$$\lambda_L^\theta \equiv \lambda_\theta = \Lambda_L + (\lambda_w + R_2) - R_1 = \lambda_w(1-\bar{\beta}_x) + \lambda_w(1-\cos\theta) =$$
$$= \lambda_w(2-\bar{\beta}_x-\cos\theta) \cong \lambda_w(1-\bar{\beta}_x\cos\theta),$$

where λ_L coincides with the resonant radiation wavelength $\lambda_R = \lambda_w(1-\bar{\beta}_x)$. The values of λ_θ and ω_θ may be obtained in a more exact form making use of the expression of λ_R given by eq. (2.5):

$$\lambda_\theta \cong \lambda_w(1+a_w^2)/2\gamma^2 + \lambda_w\theta^2/2, \qquad \omega_\theta \cong 2\omega_w\gamma^2/(1+a_w^2+\gamma^2\theta^2).$$

The analytical results (derived from eq. (6.1)) obtained using eq. (5) of ref. [4] are shown in fig. 17. The spectral bandwith of each line (*i.e.* the linewidth factor $\Delta\omega/\omega$) is of the order of $1/N$ (normally for an undulator, $N \cong 60$, in this calculation, $N = 7$).

We show in fig. 18 the results obtained by means of our numerical procedure in the case of a single particle: by comparison with fig. 17 a good agreement is found with the analytical results.

We feel therefore reasonably induced to believe in the numerical results obtainable in the case of the radiation due to a system of many particles, as required by the treatment of the bunches of an entire FEL. With respect to the case of single-particle radiation, the radiation due to a system of particles placed at resonant mutual distances turns out to contain a smaller number of higher harmonics and to be confined, because of the destructive interference effects, within a smaller solid angle around the FEL axis (fig. 19*a*), *b*)). Due to the interference effects between the radiations of many particles, the overall radiation spectrum resembles therefore the ideal case of a coeherent monocromatic laser much more than the spectrum of a single charge.

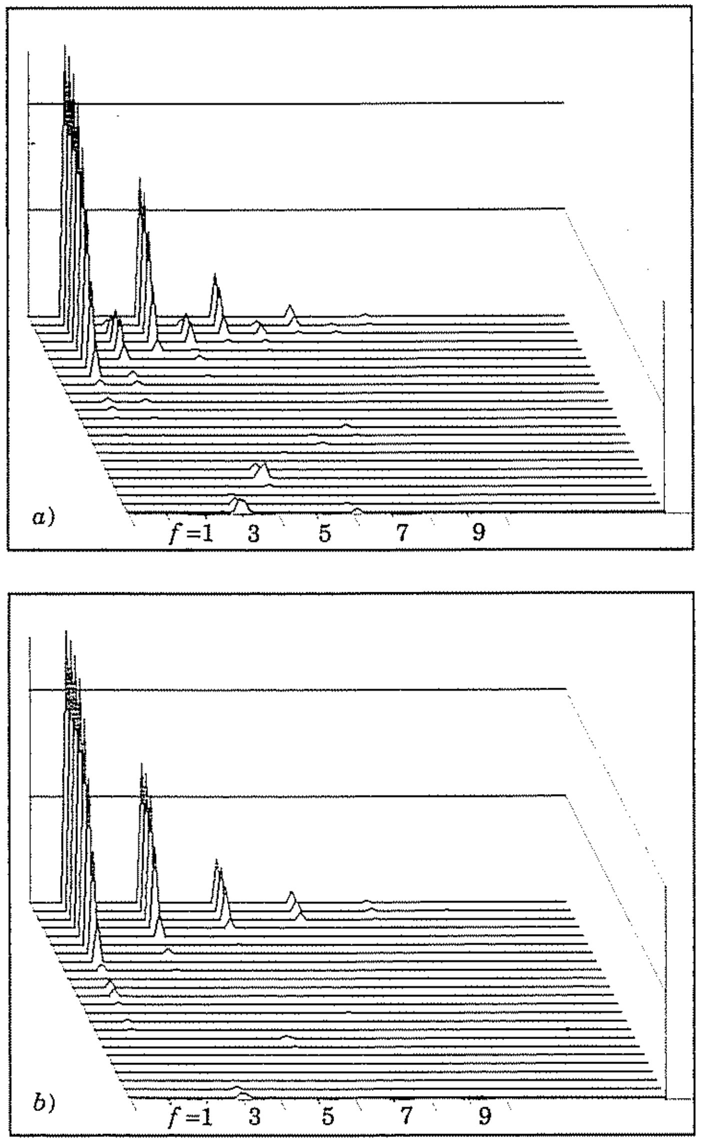

Fig. 19. – Spectral analysis analogous to fig. 17 and 18, taking however into account the radiation due to 14 charges, placed at resonant mutual distance. The radiation is collected on a screen at 300 cm from the first radiating charge. The planes of the observation angles are perpendicular and parallel, respectively, to the wiggler magnetic field in *a*) and *b*).

7. – Conclusions.

In the current literature the radiation of an FEL is generally analysed in stationary conditions, making use of expression (6.1) of the spectral density angular distribution, which does not explicitly contain the acceleration $\dot{\beta}$ of the radiating particle, and where both the trajectory and the velocity of each bunch must

be *a priori* assigned. Such a stationary state corresponds to a set of bunches filling the entire length of the FEL.

The mutual interactions between the bunches cause a small, almost stationary perturbation in the motion of a single test bunch (or electron). In the present work the aforementioned limitations were avoided making directly use of the motion equations of the considered bunches, and keeping into account the non-stationary radiation terms, provided by the well-known Lienard-Wiechert potentials.

Although our approach lends itself to the treatment of the motion of a limited number of bunches, the total field acting on the test particle is quite realistic, since the presence of a larger number of bunches in resonant conditions would only change the strength of the wave field, and not its phase.

The overall wave front is obtained for an arbitrary radiation angle, and the spectral frequency distribution is shown to coincide, in the particular case of a single isolated radiating particle, with a well-known analytical one [4].

The oscillation of a test charge around its resonant equilibrium position may also be obtained by means of our approach, and turn out to coincide with the results of the standard treatments.

Interference effects, arising from the sum of the radiation of many bunches, were found to be responsible for the narrow-angle radiation patterns obtained, and for the resulting high degree of monochromaticity of actual radiated field.

Note added in proofs.

After having completed the present work the Author found out the existence of a paper by Elias and Gallardo [13] based on a quite similar approach. In such a paper, however, the mutual (both electrostatic and radiative) interaction between the FEL bunches is not taken into account, and it is our opinion that such an interaction significantly contributes to the highly transient phenomena of the FEL dynamics.

* * *

Thanks are due to Prof. A. Orefice (Università di Milano) for his help along the genesis of the present work.

REFERENCES

[1] Barbini R. *et al.*, *Riv. Nuovo Cimento*, **13**, No. 6 (1990).
[2] Bonifacio R. *et al.*, *Riv. Nuovo Cimento*, **13**, N. 9 (1990).
[3] Giovanelli R., *Nuovo Cimento D*, **15** (1993) 39.
[4] Colson W. B., *IEEE J. Quantum Electron.*, QE-17 (1981) 1417; PhD dissertation, Stanford University (1977).
[5] Brau C. A., *Free-Electron Lasers* (Academic Press) 1990.
[6] Landau L. and Lifschitz E., *Theorie du champ* (MIR, Moscou) 1966.
[7] Jackson J. D., *Classical Electrodynamics* (J. Wiley) 1975.
[8] Leubner C. and Ritsch H., *Nucl. Instrum. Methods A*, **246** (1986) 45.
[9] Kim K., *Nucl. Instrum. Methods A*, **246** (1986) 71.
[10] Rarback H. *et al.*, *Nucl. Instrum. Methods A*, **266** (1988) 96.
[11] Wigner E., *Phys. Rev.*, **40** (1932) 749.
[12] Kincaid B. M., *J. Appl. Phys.*, **48** (1977) 2684.
[13] Elias L. R. and Gallardo J. C., *Phys. Rev. A*, 24 (1981) 3276.